

# Quantum to Classical Walk Transitions Tuned by Spontaneous Emissions

J. H. Clark,<sup>1</sup> C. Groiseau,<sup>2,3</sup> Z. N. Shaw,<sup>1</sup> S. Dadras,<sup>4</sup> C. Binegar,<sup>1</sup> S. Wimberger,<sup>5,6,\*</sup> G. S. Summy,<sup>1,†</sup> and Y. Liu<sup>1,‡</sup>

<sup>1</sup>*Department of Physics, Oklahoma State University, Stillwater, Oklahoma 74078, USA*

<sup>2</sup>*Dodd-Walls Centre for Photonic and Quantum Technologies, New Zealand*

<sup>3</sup>*Department of Physics, University of Auckland, Auckland 1010, New Zealand*

<sup>4</sup>*TOPTICA Photonics Inc., 5847 County Road 41, Farmington, New York 14424, USA*

<sup>5</sup>*Dipartimento di Scienze Matematiche, Fisiche e Informatiche, Università di Parma, Campus Universitario, Parco area delle Scienze 7/a, 43124 Parma, Italy*

<sup>6</sup>*INFN - Sezione di Milano-Bicocca, gruppo collegato di Parma, Parco Area delle Scienze 7/A, 43124 Parma, Italy*

(Dated: August 23, 2021)

We have realized a quantum walk in momentum space with a rubidium spinor Bose-Einstein condensate by applying a periodic kicking potential as a walk operator and a resonant microwave pulse as a coin toss operator. The generated quantum walks appear to be stable for up to ten steps and then quickly transit to classical walks due to spontaneous emissions induced by laser beams of the walk operator. We investigate these quantum to classical walk transitions by introducing well-controlled spontaneous emissions with an external light source during quantum walks. Our findings demonstrate a scheme to control the robustness of the quantum walks and can also be applied to other cold atom experiments involving spontaneous emissions.

## I. INTRODUCTION

Quantum walks (QWs) have been actively studied in many experimental systems, such as photons, lattice-confined atoms, and trapped ions, since the first theoretical model was introduced in 1993 [1–7]. Possessing spin degrees of freedom, spinor Bose-Einstein Condensates (BECs) have also been suggested as ideal candidates for QW implementation [8]. Two important components of QWs are a walk operator to shift a walker in positions or momentum space and a coin toss operator to determine the direction that the walker shifts in each step [9]. In this work, a rubidium spinor BEC subjected to a series of periodic optical pulses, which can be described as an atom-optics kicked rotor (AOKR), is utilized to create a QW in momentum space [10–13]. These periodic pulses construct one-dimensional (1D) optical lattices and act as a walk operator in momentum space. Resonant microwave pulses, entangling two hyperfine spin states, are the coin toss operator. In contrast to classical random walks with Gaussian distributions, QWs distribute ballistically because atoms conducting QWs can be in a superposition state [1, 10, 11]. Other advantages of QWs studied in this paper include hitting target points faster than classical walks, fast propagation, and entanglement between internal and external degrees of freedom [1, 14]. QWs thus have many proposed and realized applications in various research fields including quantum information, metrology, and topological phenomena [15].

In this work, we demonstrate that our quantum walk in momentum space can be stable for up to ten steps and then quickly transit to classical walks due to spontaneous

emission (SE) induced by the laser beams imprinting a momentum change. The SE effects have been observed in our previous experiments and are pervasive in other experiments utilizing AOKR [16, 17].

We investigate the SE-tuned quantum to classical walk transitions by introducing well-controlled SE with an additional laser which does not interfere with the kick or shift laser of our QW. Those effects are manifold since SE acts as projective measurement in the internal electronic spin degree of freedom of the atom. On the other hand, SE has the twofold effect on the external center-of-mass degree of freedom of the atoms in our BEC: first it changes the quasimomentum and hence the conditions of being in the QW or not, see [10, 11], and secondly, it biases the QW towards the direction of the ground state into which the electronic degree is projected. This is also contrary to previous experiments [16] with just one effective internal state in which SE only had an influence on the quantum-resonance condition and hence on the external degree of freedom. In our experiments, the probability of a SE event and the induced decoherence appear to increase with the evolution of time, i.e., with the number of steps in a QW. We also confirm the SE events lead to a biased momentum distribution, which agrees well with our numerical simulations. Our findings demonstrate a scheme to control the robustness of quantum walks and can also be applied to other cold atom experiments involving spontaneous emissions [18, 19].

## II. THEORETICAL PREDICTIONS

Similar to our previous works, we describe each QW step with an operator  $\hat{U}_{\text{step}} = \hat{\mathbf{T}}\hat{\mathbf{M}}$  [10, 11]. A unitary walk operator  $\hat{\mathbf{T}}$  implemented by AOKR entangles the internal (i.e., spin) and external degrees of freedom, which leads to a momentum change of  $p_m = m\hbar G$  [10–

\* Electronic address: sandromarcel.wimberger@unipr.it

† Electronic address: gil.summy1@gmail.com

‡ Electronic address: yingmei.liu@okstate.edu

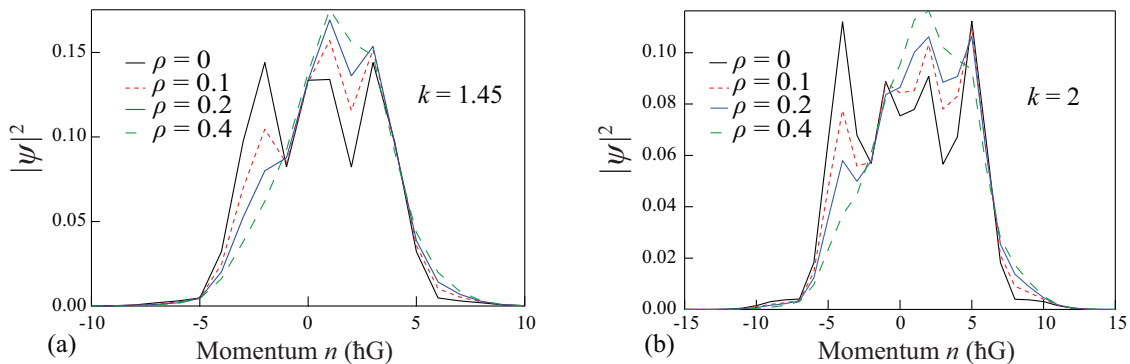


FIG. 1. Simulated momentum distributions of 5-step quantum walks at two kicking strengths,  $k = 1.45$  (a) and  $k = 2.0$  (b), averaged over  $1 \times 10^3$  trajectories with  $\Delta_\beta = 0.025\hbar G$  at various probabilities  $\rho$  of SE events. Here  $\Delta_\beta$  is the width of the quasimomentum  $\beta$ . Note the increasing asymmetry as the probability  $\rho$  increases.

13]. Here  $G$  is the wavevector of the 1D lattice,  $\hbar$  is the reduced Planck's constant, and  $m$  is an integer number. The coin operator  $\hat{M}$ , created by a microwave pulse resonant with the transition between  $|F = 1, m_F = 0\rangle$  and  $|F = 2, m_F = 0\rangle$  states of  $^{87}\text{Rb}$  atoms, produces a superposition of these two internal states. We apply a controlled amount of SE during a QW sequence using an independently controlled laser, which excites atoms from the  $|F = 2\rangle$  ground state resonantly to the  $|F' = 3\rangle$  excited state. The laser coupling  $\Omega = \gamma\sqrt{\frac{I}{2I_s}}$  is small compared to the excited state hyperfine splitting between  $|F' = 3\rangle$  and  $|F' = 2\rangle$ , so that the  $|F' = 2\rangle \rightarrow |F' = 2\rangle$  transition can be assumed to be too far detuned to create a significant population in  $|F' = 2\rangle$ . Here  $I$  is the intensity of the laser,  $I_s$  is the saturation intensity, and  $\gamma$  is the decay rate [20]. Due to selection rules, the atom can only decay from  $|F' = 3\rangle$  back to  $|F = 2\rangle$ , corresponding to a projection of the atom onto  $|F = 2\rangle$ . The SE pulse is long enough that we can assume the atom reaches the steady-state (the coin pulse should not interfere with that) meaning that the effective SE-rate  $\gamma_{\text{eff}}$  is given by the natural line width times the steady-state population of  $|F' = 3\rangle$  as follows [20],

$$\gamma_{\text{eff}} = \frac{\gamma}{2} \frac{I/I_s}{1 + I/I_s}, \quad (1)$$

from which we get the probability of an event per pulse

$$\rho = \gamma_{\text{eff}} t_{\text{SE}}. \quad (2)$$

Technically,  $\gamma_{\text{eff}}$  and  $\rho$  change during a single trajectory. The probability of the first decay overall and in each further decay has to be scaled down by a factor 2 since the atom will be either exactly or close to an equal superposition of the two ground states. So the given rate represents an upper limit, good only a couple of  $\mu\text{s}$  after an event. We estimate  $\rho \approx 0.35$  for a SE power of  $3 \mu\text{W}$  for our experimental system, as elaborated in Section-III.

Since the SE light is introduced  $30 \mu\text{s}$  after the start of the coin, SE events will interrupt the coin pulse at

random times, the partial action of the coin operator in between two events of time delay  $t$  is

$$e^{i\frac{\pi t}{4T}\hat{\sigma}_x} = \begin{bmatrix} \cos(\frac{\pi t}{4T}) & i \sin(\frac{\pi t}{4T}) \\ i \sin(\frac{\pi t}{4T}) & \cos(\frac{\pi t}{4T}) \end{bmatrix}, \quad (3)$$

where  $T$  is the total length of the coin pulse.

This means that the state of the internal degree of freedom at the end of the coin sequence is only determined by the time of the last SE event  $t' \in [0.29, 0.58] \times T$  and thus given by

$$|\psi\rangle = \cos\left[\frac{\pi(T-t')}{4T}\right]|2\rangle + i \sin\left[\frac{\pi(T-t')}{4T}\right]|1\rangle. \quad (4)$$

Here  $|1\rangle$  and  $|2\rangle$  represent the two internal states,  $|F = 1, m_F = 0\rangle$  and  $|F = 2, m_F = 0\rangle$ , respectively. Eq. (4) clearly shows that SE creates an imbalance in the internal state of the atoms towards  $|F = 2\rangle$ , which gets transferred to the populations and results in a biased momentum distribution (see our simulations in Fig. 1).

Each SE event also affects the external degree of freedom by shifting the quasimomentum  $\beta$  by a random amount. Contrary to SE induced by the kicking beams [12], the atom does not incur any recoil from the absorption of a photon from the SE beam due to its perpendicular alignment to the walk axis.

In our simulations, we draw up to 3 Poisson-distributed times and perform the partial coin operator from the largest time that is still inside the coin duration. We also add the corresponding amount of random recoil (here taken to be uniformly distributed). Typical simulation results for 5-step quantum walks at two kicking strengths  $k$  are shown in Fig. 1, which clearly show transitions from quantum walks to classic walks as the probability  $\rho$  of SE events increases.

### III. EXPERIMENTAL PROCEDURES

Each experimental sequence starts with a BEC of approximately  $4 \times 10^4$   $^{87}\text{Rb}$  atoms at the  $|F = 1, m_F = 0\rangle$  state. The BEC is then subjected to Bragg, AOKR and

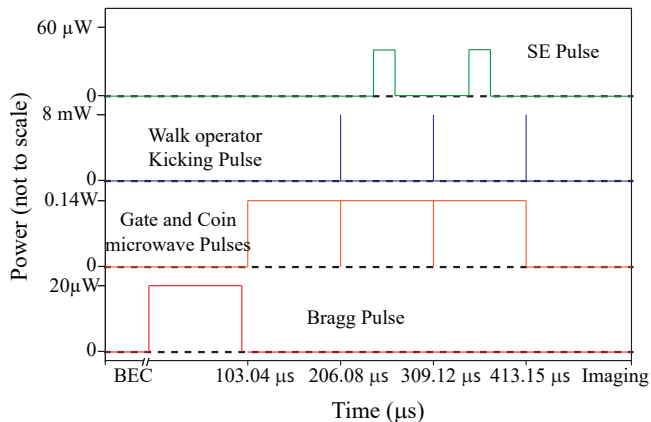


FIG. 2. Schematic diagram showing the sequence of various optical and microwave pulses used in our experiments. The time duration of each SE pulse is  $30 \mu\text{s}$ . All axes are not to scale.

microwave pulses. A schematic outlining of the pulse sequences is shown in Fig. 2. The AOKR and Bragg pulses are realized with the same two counter-propagating laser beams that intercept on the BEC, although the Bragg pulse has a longer duration to drive the BEC into the state  $|\psi_0\rangle = 1/\sqrt{2}(|n=0\rangle + e^{i\phi}|n=1\rangle)$  [10, 21]. We control populations of the two internal states  $|1\rangle$  and  $|2\rangle$  using the microwave (coin toss) pulses resonant with the  $|1\rangle$  to  $|2\rangle$  transition.

The standard QW of  $i$  number of steps is created with a sequence of pulses described by the operator  $(\hat{U}_{\text{step}})^i = [\hat{\mathbf{T}}\hat{\mathbf{M}}(\pi/2, -\pi/2)]^{i-1}[\hat{\mathbf{T}}\hat{\mathbf{M}}(\pi/2, \pi)]$ . To ensure that the QW is symmetric the first coin pulse in the sequence is a Hadamard gate, which prepares the initial internal states as  $\hat{\mathbf{M}}(\pi/2, \pi)|1\rangle = 1/\sqrt{2}(|1\rangle + |2\rangle)$ . For the standard QWs in our experiments an additional phase offset is applied to the coin microwave pulses to cancel out a global phase that acts upon the QW due to the kicking light pulses [10, 22]. A QW that has the proper phase offset is referred to as phase compensated. During the coin toss pulses a SE light with a pulse duration of  $30 \mu\text{s}$  is added to induce well-controlled SE effect onto the QW. A delta AOKR kicking pulse is then applied as the walk operator in momentum space followed by a coin toss microwave pulse. These coin toss pulses act on the internal states to entangle the internal and external degrees of freedom. This sequence of coin toss followed by a delta pulse is then repeated until QWs for  $i$  number of steps are recorded and time of flight (TOF) images are taken via the standard absorption imaging method [10, 22].

#### IV. RESULTS AND DISCUSSIONS

Figure 3 shows the effects of SE on a five step QW in which the phase of the walk is non-compensated although the phase of the microwave pulses are held constant

throughout the data run. The AOKR kicking strength during the non-compensated QWs is kept at  $k = 1.45$ , which has been proved to yield ideal QWs [10, 22]. The TOF images shown in Fig. 3(a) indicate that the population of the atoms shifts toward the positive momentum states as the power of the SE pulse increases. This observation confirms the prediction of Fig. 1, i.e., SE creates an imbalance in the internal state of the atom towards the  $|F = 2\rangle$  state, to a biased momentum distribution due to the projection of that state which is moving in the direction of positive momenta. This shift in momentum is quantitatively analyzed in Fig. 4(c). In addition, the overall population of atoms present also decreases as the SE power increases. The effective decay rate of the QW is estimated from the observed exponential atom losses as the SE power increases (see the solid lines in Fig. 3(b) and Fig. 3(c)). A typical example of our SE calibrations is shown in Fig. 3(c) which plots the condensate fraction for a BEC versus the duration of a single SE pulse of increasing duration at a fixed SE power of  $3 \mu\text{W}$ . The BEC is first prepared in  $F = 2$  before being subjected to a SE pulse of light increasing in  $50 \mu\text{s}$  intervals. The exponential fitting of this data indicates that the probability of SE event at this power is  $\rho = 0.35$ .

We repeat the above experiment with a properly compensated QW generated at a higher kicking strength of  $k \simeq 2$  to ensure that the QW distribution is broader than those created with the lower kicking strength. We scan the SE power up to  $7.2 \mu\text{W}$  with an average of eight runs per power setting. The observed distribution of the QWs does not show noticeable differences beyond this power value. Typical TOF images of the compensated QWs are shown in Fig. 4(d), which indicate that the atoms in the compensated walks also shift toward the positive momentum states as the SE power increases. The decay of the QW distribution can be more easily discerned from the momentum distributions, as displayed in Figs. 4(a) and 4(b). We also extract the mean momentum and mean energy from the non-compensated and compensated QW data, and respectively show them as a function of the SE power in Fig. 4(c) and Fig. 4(e). A positive shift in the mean momentum as the SE pulses become more powerful is confirmed in Fig. 4(c) for both compensated and non-compensated QWs. In both cases the mean momentum was initially negative due to the phase of the applied microwave coin pulses being larger than  $2\pi$  thus causing an initial bias toward negative mean momentum. For a standard QW in our experiments this phase on the coin microwave pulses is normally below  $(2k + \pi)$  to cancel out a global phase that acts upon the QW due to the kicking light pulses [10, 22]. Although this bias can adversely affect the momentum distribution of a QW that evolves in time it did not prevent the observation of the positive shift in mean momentum as the power of the SE pulses increased. This was because the same microwave coin phase was applied throughout an experiment as the SE pulse power was scanned. On the other hand, Fig. 4(e) implies that the mean energy

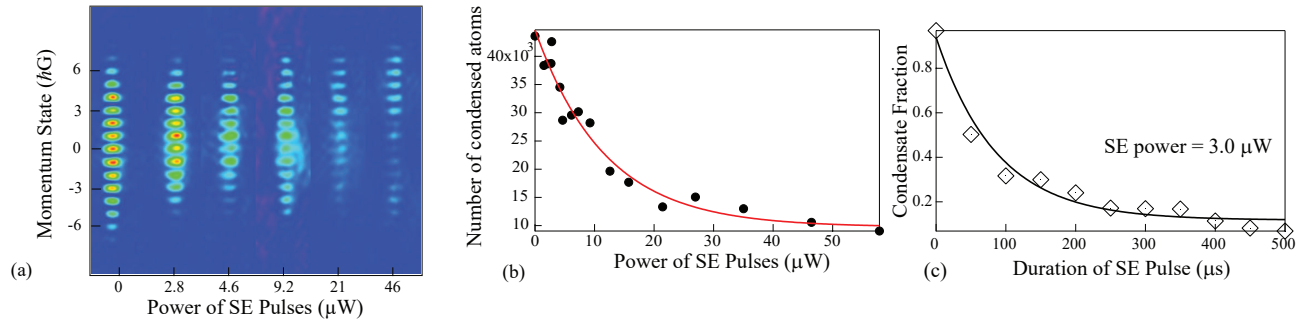


FIG. 3. (a) TOF images of a phase non-compensated five-step QW under various SE powers at the kicking strength  $k = 1.45$  and the SE pulse duration of  $30 \mu\text{s}$ . (b) The number of condensed atoms versus the SE power in the noncompensated QWs shown in Panel (a). (c) The condensate fraction versus SE pulse duration for a single BEC subjected to a pulse of SE light at  $SE = 3.0 \mu\text{W}$ . Solid lines in Panel (b) and Panel (c) are exponential fits.

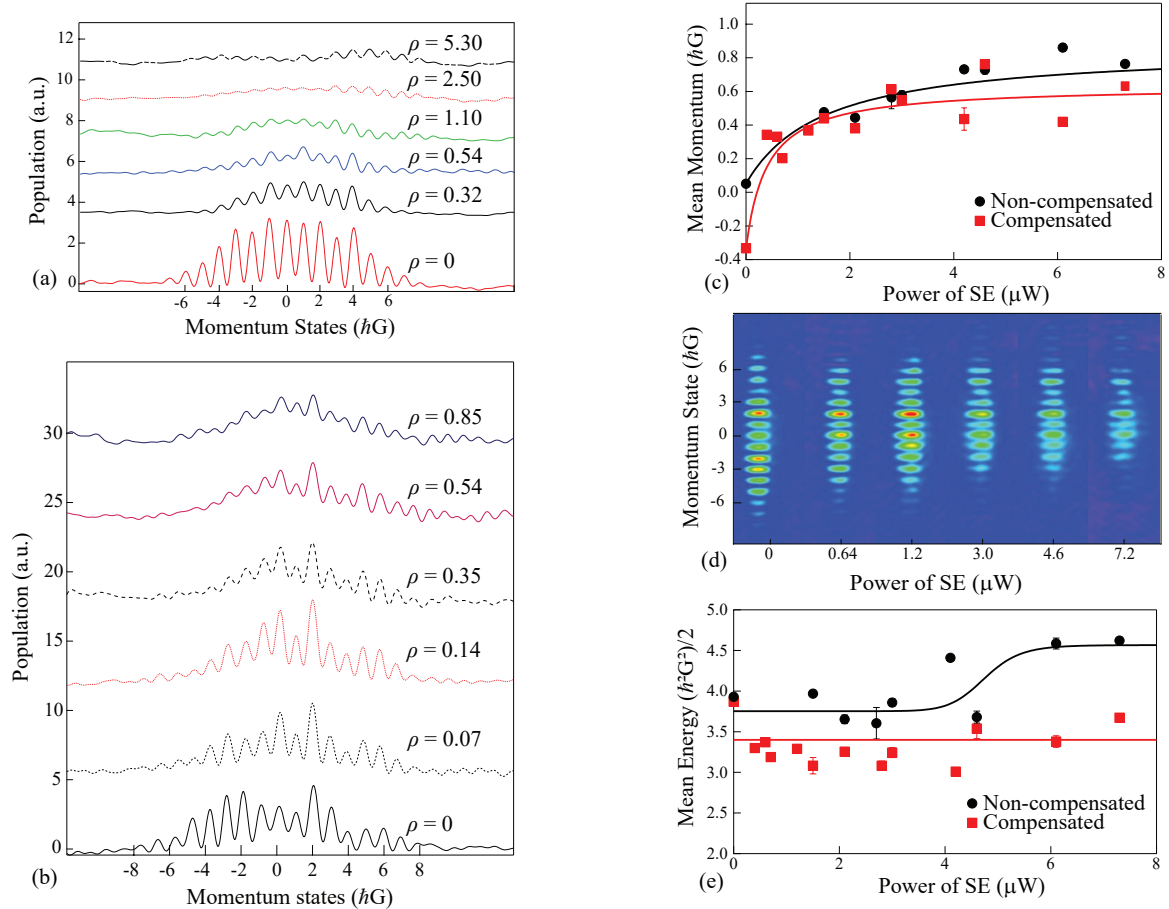


FIG. 4. Typical momentum distributions of (a) a phase non-compensated QW and (b) a phase compensated QW at various  $\rho$  and at a fixed SE pulse duration of  $30 \mu\text{s}$  (see text). Each momentum distribution is shifted by a constant offset for visual clarity. (c) The mean momentum extracted from Panels (a) and (b) as a function of the SE power. (d) Typical TOF images in the compensated QWs. (e) The mean energy extracted from Panels (a) and (b) versus the SE power. Solid lines in Panel (c) and Panel (e) are fitting curves to guide the eye.

slightly increases for the non-compensated QWs while remaining constant for the compensated QWs as the SE power increases within the range of 0 to  $7.2 \mu\text{W}$ , i.e., the SE probability is within the range of 0 to 0.85.

Our data in Fig. 3 and Fig. 4 indicate that the quan-

tum to classical walk transitions happen at around  $5 \mu\text{W}$ , much lower than the maximum SE power studied in this paper. To clearly demonstrate the transition of walks from displaying quantum to classical behaviors under the applied SE pulses, we conduct similar experiments on

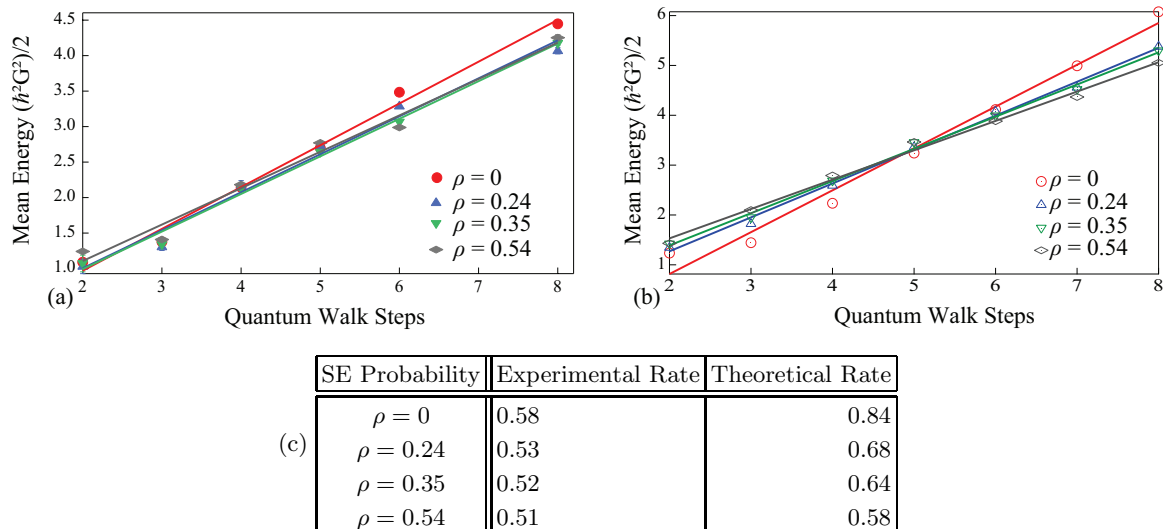


FIG. 5. (a) The extracted mean energy as a function of the QW steps at various probability  $\rho$  of SE events and  $k = 1.4$ . The difference in the mean energy among various probability  $\rho$  of SE events remains relatively constant at lower number of steps but begins to decrease at six steps, indicating a transition from a QW to a classical walk. (b) Theoretical predictions based on the experimental conditions for the data shown in Panel (a). The solid lines in both panels represent the linear fitting functions. (c) Rate  $R$  extracted from Panel (a) and Panel (b) (see text).

walks of various numbers of steps. For each step the kicking strength is kept at  $k = 1.4$  to reduce the probability of extra SE events induced by the kicking beams. The mean energy extracted from these experiments are plotted as a function of the QW steps for various probability  $\rho$  of SE events in Fig. 5(a), which shows that the mean energy increases with increasing number of steps at a rate  $R$  which depends on the applied SE power. The rate  $R$  for the zero probability  $\rho$  of SE events appears to be the largest, as shown by the red markers in Fig. 5(a). As the SE pulse is applied and becomes more powerful, the rate  $R$  gets smaller leading to an increased difference in the mean energy among data taken under various probability  $\rho$  of SE events at a high enough step, as clearly demonstrated by the 6-step and 8-step data in Fig. 5(a). These observations qualitatively agree with the theoretical predictions derived under similar conditions, as shown in Fig. 5(b). Each data set in both Fig. 5(a) and Fig. 5(b) are fit with a linear function and the rate  $R$  are calculated and tabulated in Fig. 5(c). Our observations agree well with a predicted signature for quantum to classical walk transitions, i.e., QWs have larger mean energy than classical walks at a given step because QWs distribute ballistically while classical walks follow Gaussian distributions [1, 10, 11]. Our data thus indicate that the QWs gradually transit to classical walks with less mean energy as the applied SE effect becomes powerful enough to destroy the entanglement of the two internal spin states. Figure 5 also shows that QWs are able to maintain their robustness when the number of steps is lower than five.

## V. CONCLUSIONS AND OUTLOOK

We have presented quantum to classical walk transitions tuned by spontaneous emissions. The SE rate is derived from the observed atom losses during QWs. We have demonstrated that the addition of the SE light yields quantum to classical walk transitions and leads to biased momentum distributions, which can be well explained by our numerical simulations in both the compensated and non-compensated QWs. Our findings suggest a scheme to control the robustness of the quantum walks and demonstrate that the effects of the SE light are intriguing. While a SE event acts as a projective measurement on the internal spin degree of freedom, its effect on the external motion, that is the actually observed quantity, is direct by a change of the necessary resonance conditions for the QW, but also indirect since the motion becomes biased into the direction into which the ground state likes to move. Hence, for the center-of-mass of our atoms, SE is not a strong but rather a weak form of quantum measurement, with the internal state acting as an ancilla that is actually strongly measured. Many SE events will then necessarily have a larger effect than just one SE event since they bias more the walk into one direction of the external motion. Similar ideas have been put forward, e.g., in [23]. In conclusion, our results open further possibilities of utilizing the tunable SE light to engage on the theory of measurements in experimentally easily accessible quantum systems.

**Acknowledgments** We thank the Noble Foundation for financial support.

- 
- [1] Wang, J., and Manouchehri, K. Physical Implementation of Quantum Walks *Springer* (2014)
- [2] Dur, W., Raussendorf, R., Kendon, V., and Briegel, H.-J. Quantum walks in optical lattices, *Phys. Rev. A* **66**, 052319 (2002)
- [3] Eckert, K., Mompert, J., Birkel, G., and Lewenstein, M. One- and two-dimensional quantum walks in arrays of optical traps, *Phys. Rev. A* **72**, 012327 (2005)
- [4] Schmitz, H., Matjeschk, R., Schneider, C., Glueckert, J., Enderlein, M., Huber, T., and Schaetz, T. Quantum walk of a trapped ion in phase space, *Phys. Rev. Lett.* **103**, 090504 (2009)
- [5] Karsk, M., Forster, L., Choi, J., *et al.* Quantum walk in position space with single optically trapped atoms, *Science* **325**, 174-177 (2009)
- [6] Aharonov, Y., Davidovich, L., and Zagury, N. Quantum Random Walks, *Phys. Rev. A* **48**, 1687 (1993)
- [7] Alberti, A., and Wimberger, S. Quantum walk of a Bose-Einstein condensate in the Brillouin zone, *Phys. Rev. A* **96**, 023620 (2017)
- [8] Chandrashekar, C. M., Implementing the one-dimensional quantum (Hadamard) walk using a Bose-Einstein condensate, *Phys. Rev. A* **74**, 032307 (2006)
- [9] Kempe, J., Quantum random walks-an introductory overview, *Contemp. Phys.* **44**, 4 (2003)
- [10] Dadras, S., Gresch, A., Groiseau, C., Wimberger, S., and Summy, G. S., Experimental realization of a momentum-space quantum walk, *Phys. Rev. A* **99**, 043617 (2019).
- [11] Dadras, S., Gresch, A., Groiseau, C., Wimberger, S., and Summy, G. S., Quantum Walk in Momentum Space with a Bose-Einstein Condensate, *Phys. Rev. Lett.* **121**, 070402 (2018).
- [12] Groiseau, C., and Wimberger, S., Spontaneous emission in quantum walks of a kicked Bose-Einstein condensate, *Phys. Rev. A* **99**, 013610 (2019).
- [13] Shenvi, N., Kempe, J., and Birgitta Whaley, K., Quantum random-walk search algorithm, *Phys. Rev. A* **67**, 052307 (2003)
- [14] Portugal, R., Quantum Walks and Search Algorithms, *Springer* (2018)
- [15] Asboth, J. K., Symmetries, topological phases, and bound states in the one-dimensional quantum walk, *Phys. Rev. B* **86**, 195414 (2012)
- [16] d'Arcy, M. B., Godun, R. M., Summy, G. S., Guarneri, I., Wimberger, S., Fishman, S., and Buchleitner, A., Decoherence as a probe of coherent quantum dynamics, *Phys. Rev. E* **69**, 027201 (2004).
- [17] Shrestha, R. K., Ni, J., Lam, W. K., Summy, G. S., and Wimberger, S., Dynamical tunneling of a Bose-Einstein condensate in periodically driven systems, *Phys. Rev. E* **88**, 034901 (2013)
- [18] Chai, S. and Andersen, M. F., Enhancing survival resonances with engineered dissipation, *Phys. Rev. Research* **2**, 033194 (2020)
- [19] Chai, S., Fekete, J. and Andersen, M. F., Measuring the local gravitational field using survival resonances in a dissipatively driven atom-optics system, *Phys. Rev. A* **98**, 063614 (2018)
- [20] D. A. Steck, Rubidium 87 D Line Data (2001).
- [21] Torii, Y., Suzuki, Y., Kozuma, M., Sugiura, T., Kuga, T., Deng, L., and Hagley, E. W., Mach-Zehnder Bragg interferometer for a Bose-Einstein condensate, *Phys. Rev. A* **61**, 041602(R) (2000)
- [22] Dadras S., Discrete-time quantum walk of a Bose-Einstein condensate in momentum space, *PhD Thesis* (2018)
- [23] B. Tamir and E. Cohen, Introduction to Weak Measurements and Weak Values, *Quanta* **2**, 7 (2013)